Advanced Energy Conversion Materials
http://ojs.wiserpub.com/index.php/AECM/

UNIVERSAL WISER PUBLISHER

Research Article

Comparative Analysis Using SCAPS-1D Software on the Stability and Toxcity of the Perovskites $FAPbI_3$, and $FASnI_3$

Touré Sékou[1], Amal Bouich[1,2], Youssouf Doumbia[1,3*], Bernabé Marí Soucase[1]

[1]Institute of Design for Manufacturing and Automated Production, Polytechnic University of Valencia, Valencia, Spain
[2]Applied Physics for Aeronautical and Naval Engineering & Institute of Solar Energy, Polytechnic University of Madrid, Spain
[3]Peleforo Gon Coulibaly University of Korhogo, Korhogo, Ivory Coast
Email: doumbiayoussouf59@yahoo.fr

Received: 22 August 2024; **Revised:** 14 October 2024; **Accepted:** 14 October 2024

Abstract: Hybrid organometallic perovskites such as $FAPbI_3$ (formamidinium lead iodide) and $FASnI_3$ (formamidinium tin iodide) are recognized as promising materials for the next generation of high-efficiency solar cells. $FAPbI_3$ is particularly valued for its stability and excellent optoelectronic properties. However, the toxicity of lead and the resulting environmental concerns drive the search for alternatives like $FASnI_3$, where tin, a less toxic and more abundant element, replaces lead, which is the objective of this study. The lead-free structure simulated using SCAPS-1D software is as follows: FTO/TiO_2/$FASnI_3$/Spiro-OMeTAD/Ag. We opted for TiO_2 as the ETL due to its wide bandgap (~3.2 eV for the anatase phase), which effectively blocks holes and prevents their recombination with electrons, thus promoting better charge separation. Moreover, the favorable energy level alignment of TiO_2 with the perovskites facilitates the transfer of electrons to the silver (Ag) electrode. For the HTL, we chose Spiro-OMeTAD, whose valence band level is well aligned with that of the perovskites, making it easier to extract holes to the upper silver electrode. Using the SCAPS-1D simulator, we then compared the electrical and optical properties of the devices, focusing on key parameters such as short-circuit current density (Jsc), open-circuit voltage (Voc), fill factor (FF), and power conversion efficiency (PCE). The best results obtained after optimizing the aforementioned parameters are Jsc of 30.65 mA/cm^2 , Voc of 0.8469 V, FF of 86.63%, and PCE of 22.49%. The research presented here shows that optimizing several parameters can achieve a power conversion efficiency (PCE) of 22.49%. Additionally, the structure studied in this article could be a good candidate for future research on lead-free perovskite solar cells.

Keywords: lead-free perovskite solar cell, SCAPS-1D, thickness, defect density, power conversion efficiency, $FASnI_3$, $FAPbI_3$

Abbreviation

PCE	Power Conversion Efficiency
Jsc	Short-Circuit Current Density
U_n	Electron recombination rate
U_p	Hole recombination rate
G_n	Electron generation rate

DOI: https://doi.org/10.37256/aecm.5220245549

G_p	Hole generation rate
J_n	Electron current density
J_p	Hole current density
q	Elementary charge (charge of an electron or hole)
$p(x)$	Hole concentration as a function of position (x)
$n(x)$	Electron concentration as a function of position (x)
μ_n	Electron mobility
μ_p	Hole mobility
$E(x)$	Electric field as a function of position (x)
D_n	Electron diffusion coefficient
D_p	Hole diffusion coefficient
ε	Permittivity of the material
$p_{nt}(x)$	Trapped hole concentration as a function of position (x)
TEC	Trapped electron concentration
$N_D^+(x)$	Concentration of ionized donor atoms as a function of position (x)
N_A^-	Concentration of ionized acceptor atoms
Spiro-OMeTAD	2, 2', 7, 7'-Tetrakis(N,N-di-p-methoxyphenylamine)-9, 9'-spirobifluorene
TiO_2	Titanium Dioxide
ETL	Electron Transport Layer
HTL	Hole Transport Layer
FTO	Fluorine-doped Tin Oxide
Ag	Silver
FF	Fill Factor
Voc	Open Circuit Voltage

1. Introduction

Solar energy is now asserting itself as a fundamental pillar of the energy transition on a global scale, while photovoltaic technologies have undergone a meteoric evolution over the decades [1]. Silicon-based solar cells, which have long reigned supreme in the market, have set high standards for performance and reliability [2]. Nevertheless, their manufacturing cost, combined with a certain structural rigidity, reveals certain constraints. To overcome these limitations, thin-film cells such as those incorporating copper, indium, gallium and selenium (CIGS) [3], have emerged as an alternative of choice. They are characterised by their flexibility and lightness, although these advantages sometimes come at the expense of energy efficiency and longevity [4]. In this context, perovskites represent the latest major breakthrough in the field of photovoltaics. These innovative materials promise high performance. Compared to methylammonium-based perovskites ($MAPbI_3$), $FAPbI_3$ stands out with a narrower bandgap (~1.48 eV) [5], allowing for enhanced absorption of solar light within the visible spectrum [6]. Solar cells made from $FAPbI_3$ exhibit superior durability compared to those based on $MAPbI_3$, which degrade more quickly under harsh environmental conditions. The incorporation of the formamidinium cation (FA) significantly enhances their resistance to moisture and heat. Additionally, $FASnI_3$ is characterized by a bandgap of approximately 1.3 eV [7], lower than that of $FAPbI_3$, enabling more efficient absorption in the longer wavelengths of the visible spectrum [8]. Due to its outstanding optical properties and reinforced stability, $FAPbI_3$ [9] is emerging as a leading material for the next generation of perovskite solar cells, with continually improving efficiencies [10].

Perovskite solar cells (PSC) have created extraordinary joy in the scientific community due to their high efficiency, which increased from 3.8% to 25.7%, in a relatively short period between 2009 and 2021 [11]. Thanks to these very interesting properties, these characteristics make it an essential link for improving the performance of thin-film solar cells. The general formula of perovskite material is ABX_3, where A is a monovalent organic, inorganic or mixed cation, B is the divalent metal cation and X is a halogen [12]. However, the presence of lead (Pb) in this material constitutes a major obstacle. Researchers are studying different materials to replace lead. Among these, we can cite Sn, Sb, Bi, Ag

and Cu, which have the same composition as Pb and an oxidation state +2 [13]. Research focuses on Sn-based PSCs due to their narrow bandgap (1.2-1.4 eV) [14] which covers a wider range of solar spectrum. However, they are not stable due to the rapid oxidation of the Sn cation, from Sn^{2+} to Sn^{4+} in the presence of air [15]. The researchers increased the stability by adding SnF_2 [16], which reduced the Sn^{4+} caused by oxidation. Furthermore, it is revealed that Sn^{4+} is reduced to Sn^{2+} by mixing Sn powder in SnI_2 [17]. In this paper, a numerical simulation of the PSC structure was carried out to compare the performance of $FAPbI_3$ and $FASnI_3$ perovskites using a solar cell capacitance simulator (SCAPS-1D). Cell performance is optimized by analyzing the effect of absorber thickness, electron transport layer (ETL) and hole transport layer (HTL), as well as their donor densities and respective acceptors of the ETL, HTL layers and the active layer and finally the density of defects in the absorbent layer. After optimization of the parameters we obtained for the perovskite with Pb ($FAPbI_3$): PCE = 26.65%, Voc = 1.7945 V, Jsc = 26.838236 mA/cm^2 and FF = 22.12% and that without Pb ($FASnI_3$): PCE = 22.49%, Voc = 0.8469 V, Jsc = 30.65 mA/cm^2 and FF = 86.63%. The J-V current-voltage characteristic curve and the quantum efficiency (QE) curve will be optimized.

2. Methodology

The digital simulation of solar cells is essential, not only for the interpretation of measurements on more complex structures but also for choosing and optimizing the latter. Simulation programs require solving basic semiconductor equations such as Poisson's equation and electronic continuity equations [18-19]. these equations are solved numerically as shown below.

Here are the continuity equations for electrons and holes:

$$\frac{\partial J_{\mathrm{n}}}{\partial x} U_{\mathrm{n}} + G_{\mathrm{n}} = 0 \tag{1}$$

$$-\frac{\partial J_{\mathrm{p}}}{\partial x} U_{\mathrm{p}} + G_{\mathrm{p}} = 0 \tag{2}$$

For electrons and holes, the drift-diffusion equations are given as follows:

$$J_{\mathrm{n}} = \mathrm{q} n(x) \mu_{\mathrm{n}} E(x) + \mathrm{q} D_{\mathrm{n}} \frac{dn}{dx} \tag{3}$$

$$J_{\mathrm{p}} = \mathrm{q} p(x) \mu_{\mathrm{p}} E(x) + \mathrm{q} D_{\mathrm{p}} \frac{dp}{dx} \tag{4}$$

The Poisson equation is written as follows:

$$\frac{\mathrm{d}}{\mathrm{d}}\left(\frac{\mathrm{d}v}{\mathrm{dx}}\right) = -\frac{\mathrm{q}}{\varepsilon}\left[p - \mathrm{n} + \mathrm{N_D^+(x)} - \mathrm{N_A^-} + p_{\mathrm{t}}(\mathrm{x}) - \mathrm{n_t} \right] \tag{5}$$

Where G_{n}, G_{p}, U_{n}, U_{p}, J_{n} and J_{p} μ_{n}, μ_{p}, D_{n} and D_{p} are respectively the rates of photogenerated electron-hole pairs, the recombination rates of electrons and holes, the current densities of electrons and holes, the mobilities of electrons and holes, as well as the diffusion constants of electrons and holes. Free electrons and holes are represented by p and n respectively, q is the electronic charge, and v is the electrostatic potential. In this article, the structures of perovskite solar cells (PSC) used are FTO/TiO_2 /$FASnI_3$ /Spiro-OMeTAD/Ag and FTO/TiO_2 /$FAPbI_3$ /Spiro-OMeTAD/Ag. Here, FTO is used as forward transparent conduction oxide (TCO), $FAPbI_3$ and $FASnI_3$ are used as absorbers for leaded and lead-free perovskites respectively, TiO_2 is used as ETL, Spiro-OMeTAD is used as HTL and Ag is used as a back contact. Figure 1a shows the basic structure of the device, while Figure 1b depicts the energy bands for all layers of the

PSC. Light incident on the ETL side of the structure is absorbed by the lead-free perovskite material, and from there electrons and holes flow from the absorber to ETL and HTL, respectively. We then compared these results.The various simulation parameters for the $FASnI_3$ and $FAPbI_3$ cells are shown in Table 1.

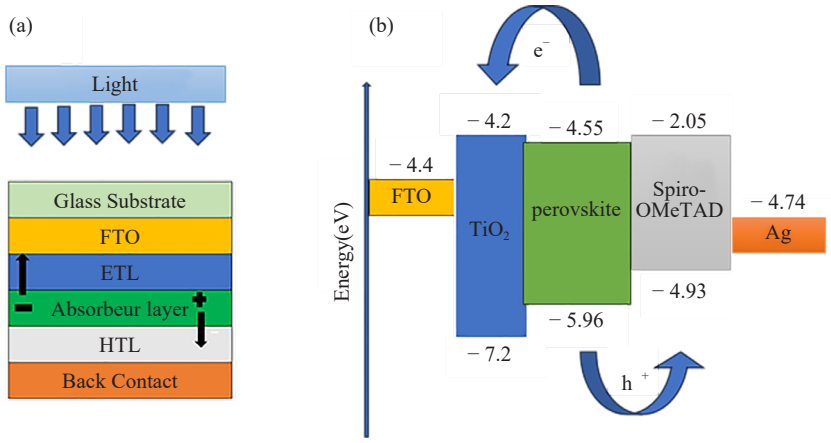

Figure 1. The basic structure of the perovskite (a) and the energy bands for all layers of the PS

Table 1. simulation parameters

parameters	Spiro: Ome-TAD [13, 25, 27]	$FASnI_3$ [13, 28]	$FAPbI_3$ [21-26]	TiO_2 [20, 27, 29]	FTO [12, 27]
Thickness (µm)	0.2	1	0.8	0.01	0.5
Bandgap (eV)	3	1.41	1.5	3.2	3.5
Electron affinity (eV)	2.2	3.52	4	4.2	4
Dielectric permittivity	3	8.2	6.6	9	9
CB effective density of states ($1/cm^{-3}$)	2.2×10^{18}	10^{18}	1.2×10^{19}	2.1×10^{18}	2.2×10^{18}
VB effective density of states ($1/cm^{-3}$)	1.8×10^{19}	10^{18}	2.9×10^{18}	10^{19}	1.8×10^{19}
Electron thermal velocity (cm/s)	10^7	10^7	10^7	10^7	10^7
Hole thermal velocity (cm/s)	10^7	10^7	10^7	10^7	10^7
Electron mobility ($cm^2/V.s$)	2.1×10^{-3}	22	2.7	20	20
Hole mobility ($cm^2/V.s$)	2.16×10^{-3}	22	2.8	10	10
Donor density N_D ($1/cm^3$)	0	0	0	10^{21}	2×10^{19}
Acceptor density N_A ($1/cm^3$)	10^{21}	10^{21}	10^{17}	0	0
		Defect parameters			
Defect type	Neutral	Neutral	Neutral	Neutal	
Capture cross section electrons (cm^2)	10^{-15}	2×10^{-15}	2×10^{-15}	10^{-15}	
Capture cross section holes (cm^2)	10^{-15}	2×10^{-15}	2×10^{-15}	10^{-15}	
Energetic distribution	Single	Gaussian	Gaussian	Single	
Energy level with respect to eV	0.1	0.5	0.6	0.6	
Characteristic energy (eV)	-	0.1	0.1	-	
Total defect density Nt (cm^{-3})	10^{15}	10^{-14}	10^{-14}	10^{14}	
Metal work function (eV)			5.125		

3. Results and discussions

3.1 *Effect of the thickness of the $FASnI_3$ and $FAPbI_3$ absorbers*

To analyze the effect of the absorber on the PSC performance, we varied the thickness of the absorber from 100 nm to 1,000 nm. It can be noted that the short-circuit current Jsc and power conversion efficiency PCE in Figures 2a and 2c respectively have the same form of evolution. The Jsc increases from 14.05 mA/cm^2 to 29.98 mA/cm^2 for $FASnI_3$ and 12.26 mA/cm^2 to 27.62 mA/cm^2 for $FAPbI_3$. This increase in Jsc and PCE is due to better absorption of photons, which increases the carrier generation rate. We note a decrease in the open circuit voltage Voc (Figure 2b) from 2.7 V to 1.47 V then an increase in the filling factor FF (Figure 2d) from 35.83% to 60.35% for $FAPbI_3$. The decrease in Voc is due to the increase in series resistance with the increase in the thickness of the absorber. The characteristics of Voc and FF (Figures 2b and 2d respectively) remain constant for $FASnI_3$ whatever the thickness value. The open circuit voltage (Voc) and the form factor (FF) remain constant despite the increase in the thickness of the $FASnI_3$ absorption layer , which is probably explained by a saturation of the effects related to light absorption, combined with recombination mechanisms that remain unchanged. In other words, the thickness of the absorption layer is already sufficient to capture all available photons, and any further increase in this thickness does not bring any improvement in the performance of the device, according to the parameters analyzed.

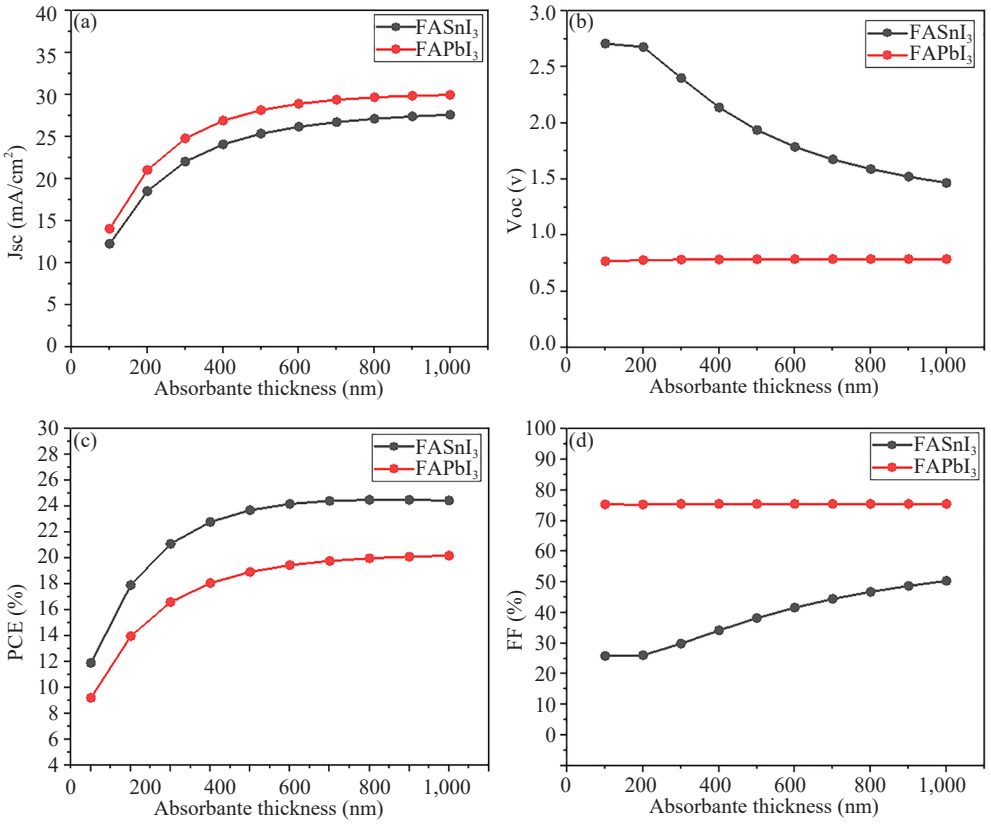

Figure 2. PSC performance as a function of absorber thickness (a) Jsc, (b) Voc, (c) PCE and (d) FF

3.2 *Effect of the thickness of the ETL electron transport layers (TiO_2) and the HTL hole transport layers (Spiro-OMeTAD)*

TiO_2 is used as ETL and Spiro-OMeTAD is used as HTL. Because of its exceptional electronic transmission capacity and long-term stability in PSCs, titanium dioxide (TiO_2) is frequently used as an electron transport layer (ETL)

in perovskite solar cells (PSC) [30]. The thickness of the TiO_2 electron transport layer (ETL) can be used to control light interference within the cell structure from an optical point of view [31]. We found that the thickness of the ETL and HTL layers have no effect on cell performance (Figures 3 and 4). The photogeneration of carriers in this layer is minimal because of their very high gap of 3.2 eV for TiO_2 and 3 eV for Spiro-OMeTAD compared to those of the absorbing layer which is 1.41 eV for $FASnI_3$ and 1.5 eV for $FAPbI_3$. These layers are used to make the junction with the absorber.

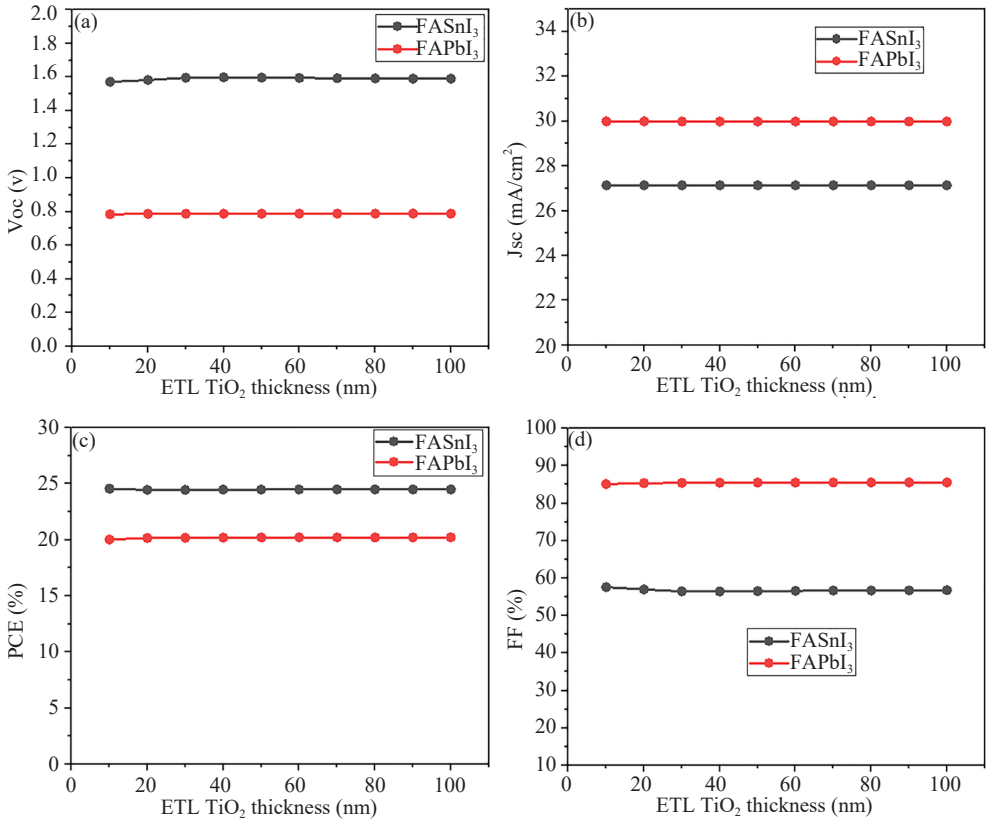

Figure 3. PSC performance as a function of ETL thickness (a)Voc, (b) Jsc, (c) PCE and (d) FF

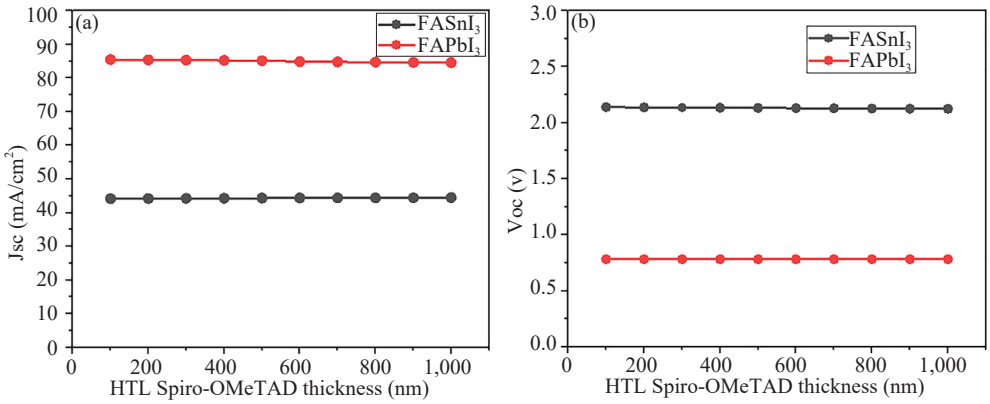

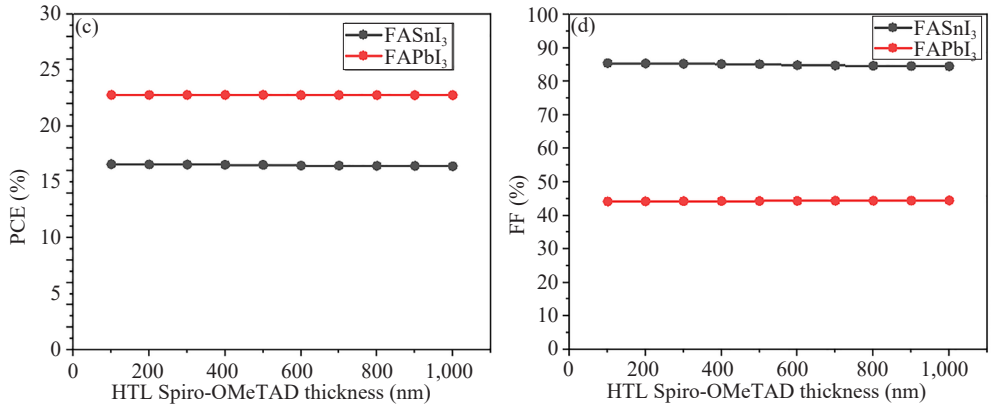

Figure 4. PSC performance as a function of HTL thickness (a) Jsc, (b) Voc, (c) PCE and (d) FF

3.3 *Effect of N_A acceptor density (cm^{-3}) of the absorbent layer*

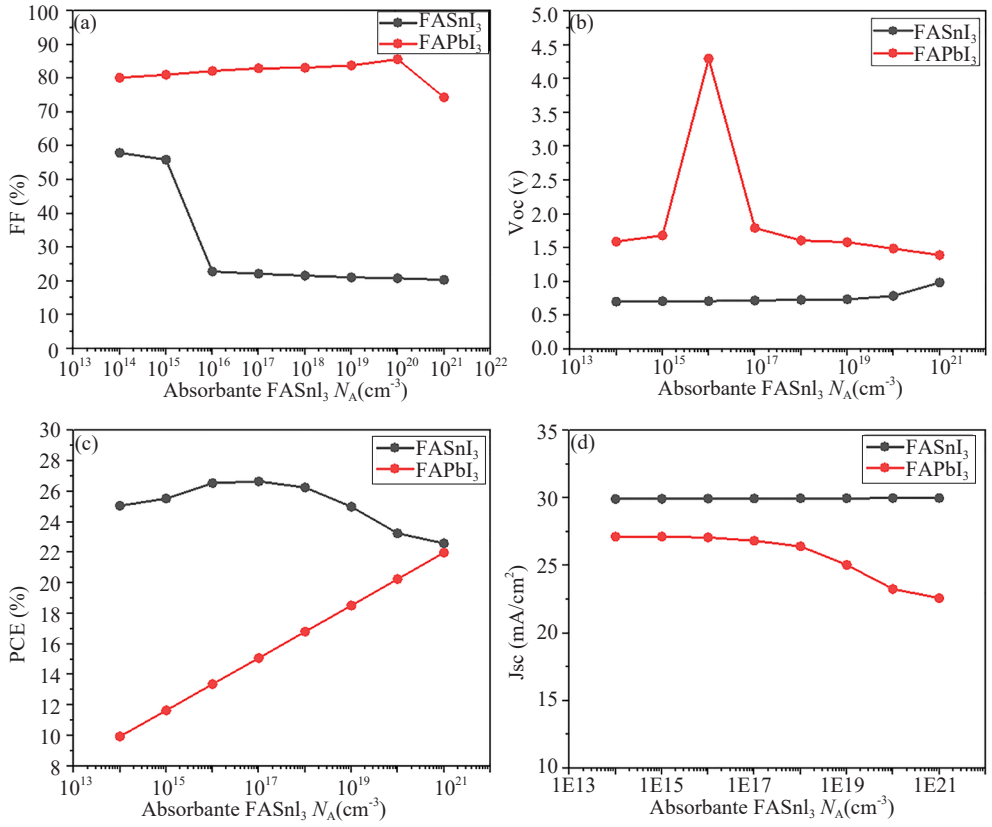

Figure 5. Effect of acceptor doping in absorber on device performance (a) FF, (b) Voc, (c) PCE & (d) Jsc

Figure 5 illustrates the evolution of photovoltaic (PV) characteristics as a function of the doping concentration in the absorbing layers, which varied from 10^{14} cm^{-3} to 10^{21} cm^{-3}. It was observed that the FF, Jsc, and Voc remain unaffected by N_A doping, leading to a rapid increase in the PCE of $FASnI_3$ from 9.20% to 20.19%. This demonstrates that PCE improves when the absorbing layer is heavily doped ($N_A = 10^{21}$ cm^{-3}), a result attributed to enhanced photon absorption. However, for doping levels exceeding 10^{17} cm^{-3}, the PCE of $FAPbI_3$ gradually decreases. In Figure 5b,

the sudden rise in open-circuit voltage (Voc) observed when the defect density reaches 10^{16} cm^{-3} is explained by a significant reduction in non-radiative recombinations and a marked improvement in the electronic properties of the absorbing layer. This development allows for better accumulation and more efficient collection of minority carriers, thereby contributing to an overall improvement in the system's performance.

3.4 *Effect of donor density N_D (cm^{-3}) ETL (TiO_2)*

To carry out the effect of the ETL layer we varied the donor density of 10^{14} cm^{-3} to 10^{21} cm^{-3}. As a result, we note that the efficiency of the device reaches a maximum value of 26.65% and 22.49% for $FAPbI_3$ and $FASnI_3$ respectively at a doping density of 10^{14} cm^{-3}, as shown in Figure 6a. In addition, VOC, JSC and FF vary very little as indicated in Figure 6 (b, c, d). Taking into account the manufacturing time, 10^{17} cm^{-3} was chosen for the ETL layer.

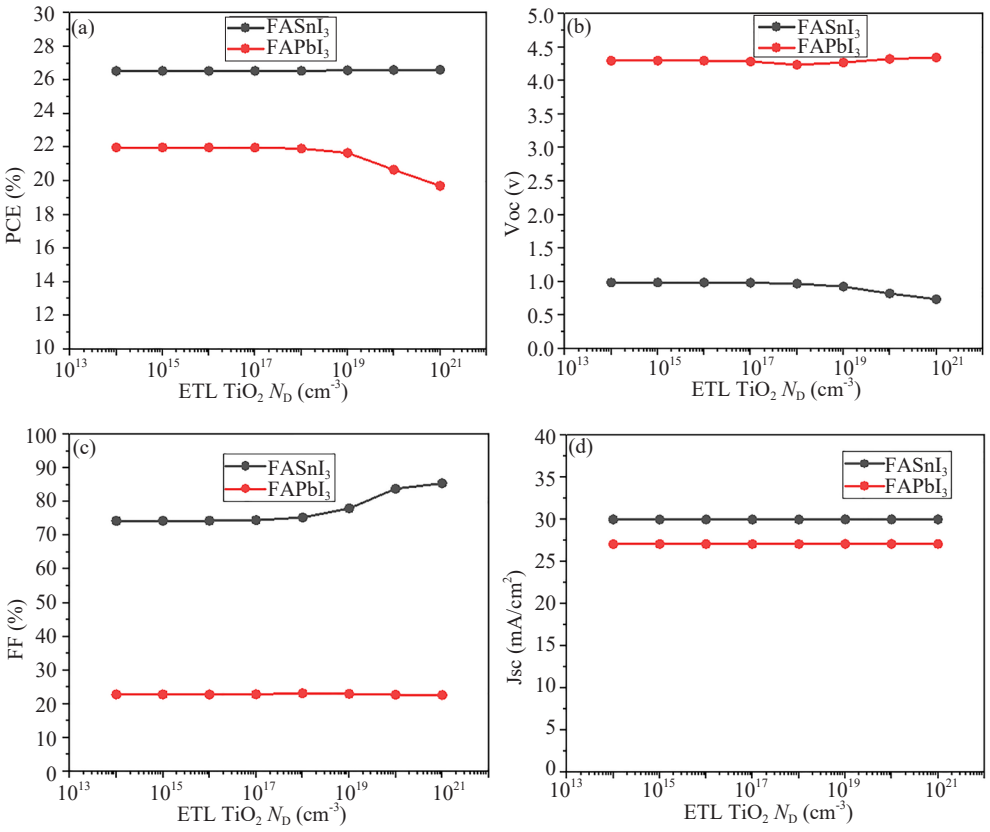

Figure 6. Influence de la densité de donneur de la couche ETL sur les performances du dispositif (a) PCE, (b) Voc (c) FF & (d) Jsc

3.5 *Effect of N_A acceptor density (cm^{-3}) HTL (Spiro-OMeTAD)*

The acceptor density of the HTL layer varies from 10^{14} cm^{-3} to 10^{21}. We see a progressive increase in the PCE of both $FASnI_3$ and $FAPbI_3$ cells (Figure 7c). This is due to the increase in the conductivity of the solar cells and also the fact of reducing the series resistance. We conclude that the optimal value to obtain a maximum PCE of the HTL layer is 10^{21} cm^{-3}. In Figure 7b the sudden increase in the open circuit voltage (Voc) observed at a defect density of 10^{17} cm^{-3} in $FASnI_3$ is attributed to a reduction in recombination losses, improvements in electronic properties, and an effect of recombination saturation. These combined factors enhance the efficient separation and collection of charge carriers, leading to an increase in Voc. The sudden decrease in the factor of form (FF) of $FASnI_3$ shown in Figure 7d at a acceptor density of 10^{17} cm^{-3} is primarily attributed to an increase in non-radiative recombination, higher internal resistances, and charge carrier trapping. These combined factors result in a loss of efficiency in the collection of carriers,

thereby reducing the overall FF of the device.

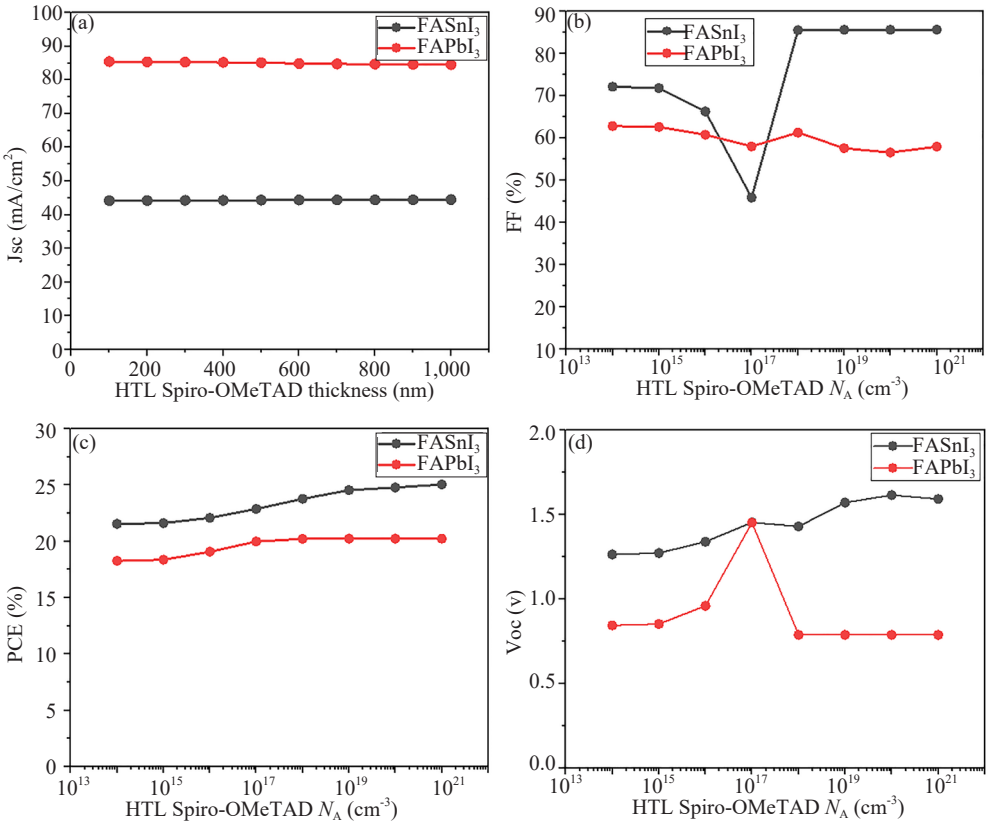

Figure 7. Influence of the acceptor density of the ETL layer on the performance of the device (a) Jsc, (b) FF (c) PCE & (d) Voc

3.6 *Effect of defect density Nt (cm^{-3}) of the absorbent layer*

Defects are inevitable in the absorbent layers, and they exist in the volume and on the surface, point defects such as gaps, interstitial defects [32]. Defects can cause deep trapping sites in the absorbent layer of the device, increasing the recombination rate [33]. When the defect density is 10^{14} cm^{-3}, the cell performance is improved and takes the maximum values. The effects of absorber doping defect density on device performance are shown in Figure 8. Figure 8a shows the effect on the JSC current density of the cells. Figure 8b shows the effect on the cell form factor FF. Figure 8c shows the effect on the PCE and figure 8d shows the effect of the absorber doping defect density on the short-circuit voltage VOC.

In Figure 9, the material $FASnI_3$ has a lower band gap than $FAPbI_3$, allowing it to absorb photons with lower energy, corresponding to longer wavelengths (in the near-infrared), which are less efficiently absorbed by $FAPbI_3$. This extended absorption capability of $FASnI_3$, covering a broader portion of the solar spectrum, promotes an increased generation of charge carriers (electrons and holes). As a result, when the applied voltage increases, the current density (J) generated by $FASnI_3$ exceeds that of $FAPbI_3$, due to greater production of charge carriers resulting from this enhanced light absorption. In $FAPbI_3$, non-radiative recombination of charge carriers is more significant, leading to a more rapid loss of current as the voltage increases. In contrast, $FASnI_3$ may possess electronic properties that limit these recombinations at higher voltages.

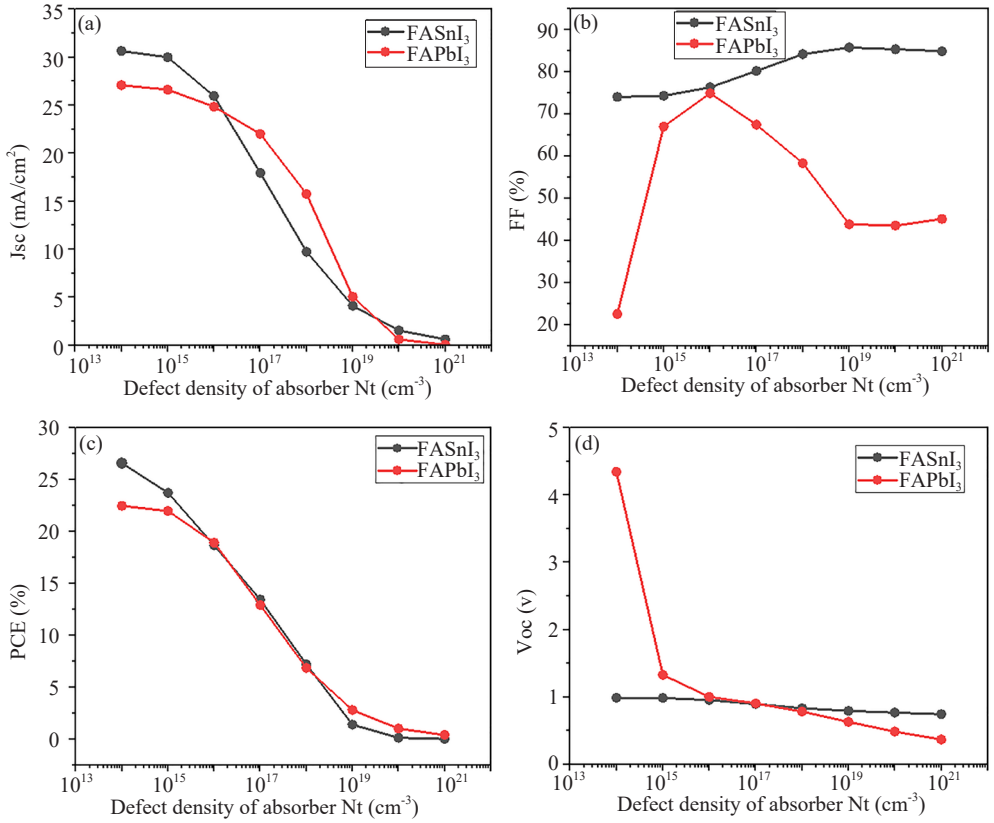

Figure 8. Effect of doping defect density of absorber on device performance (a) Jsc, (b)FF, (c) PCE, & (d) Voc

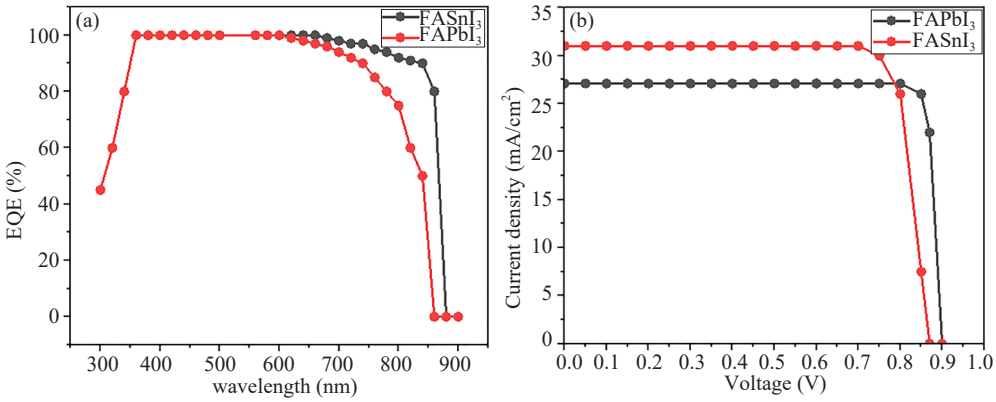

Figure 9. Characteristic curves of quantum efficiency versus wavelength(a), J-V characteristic curves of FASnI3 and FAPbI3 PSCs(b)

Table 2. Comparative parameters of $FASnI_3$ and $FAPbI_3$ perovskite solar cells

	V_{OC} (V)	J_{sc} (mA/cm^2)	FF (%)	PCE (%)
$FASnI_3$	0.8469	30.65	86.63	22.49
$FAPbI_3$	4.3481	27.09	22.59	26.61
Reference	Type of Perovskite	Interface Materials		Efficiency (%)
[34]	$FAPbI_3$	TiO_2/Spiro-OMeTAD		24.4
[35]	$FAPbI_3$	TiO_2/HTM		23.0
[36]	$FAPbI_3$	TiO_2/Spiro-OMeTAD		22.6
our work	$FAPbI_3$	TiO_2/Spiro-OMeTAD		26.61
our work	$FAPbI_3$	TiO_2/Spiro-OMeTAD		22.49

4. Conclusion

At the end of this article, we conclude that the one-dimensional solar cell simulation software SCAPS-1D used to design and simulate lead-free PSC using $FASnI_3$ as absorbent material compared to PSC with lead $FAPbI_3$ has proven to be very effective. The results obtained demonstrated that the thickness, donor and acceptor density of $FASnI_3$ have an impact on the performance of the device. We obtained the following values during the simulation: V oc = 0.8469 V, Jsc = 30.65 mA/cm^2, FF = 86.63% and PCE = 22.49%. The results of our simulations reveal that $FAPbI_3$ stands out for its remarkable power conversion efficiency (PCE), thanks to its excellent optoelectronic properties and increased stability. However, the substitution of lead with tin in $FASnI_3$ represents a promising alternative for the design of more environmentally friendly solar cells, although performance challenges with this material remain.

The optimization of several parameters, notably the thickness and doping of the electron transport layer (ETL) and hole transport layer (HTL), as well as the defect density in the absorber layer, allowed us to achieve a PCE of 22.49% for the $FASnI_3$ structure, demonstrating that this lead-free technology could compete with the performance of lead-based perovskites (Table 2). These results open promising perspectives for future research, particularly in improving tin-based materials to enhance their stability and efficiency. This approach could provide a sustainable alternative to lead-based solar cells while maintaining high energy yields.

Conflict of interest

The authors declare there is no conflict of interest at any point with reference to research findings.

References

[1] Hossain MF, Ghosh A, Al Mamun MA, Miazee AA, Al-Lohedan HA, Ramalingam RJ, et al. Design and simulation numerically with performance enhancement of extremely efficient Sb_2Se_3-Based solar cell with V_2O_5 as the hole transport layer, using SCAPS-1D simulation program. *Optics Communications*. 2024; 559: 130410. Available from: https://doi.org/10.1016/j.optcom.2024.130410.

[2] Ghosh A, Islam MS, Rahman MK, Buian MFI, Hassan A, Alrafai HA, et al. A theoretical investigation of MoS_2-based solar cells with CdS electron transport layer and V_2O_5 hole transport layer for boosting performance. *Materials Science and Engineering: B*. 2024; 307: 117521. Available from: https://doi.org/10.1016/j.mseb.2024.117521.

[3] Sonmezoglu S, Akin S. Suppression of the interface-dependent nonradiative recombination by using 2-methylbenzimidazole as interlayer for highly efficient and stable perovskite solar cells. *Nano Energy*. 2020; 76:

105127. Available from: https://doi.org/10.1016/j.nanoen.2020.105127.
[4] Reza MS, Rahman MF, Kuddus A, Mohammed MKA, Pal D, Ghosh A, et al. Design and optimization of high-performance novel $RbPbBr_3$-based solar cells with wide-band-gap S-chalcogenide electron transport layers (ETLs). *ACS Omega*. 2024; 9(18): 19824-19836.
[5] Rahman MA, Rahman MF, Marasamy L, Mohammed MKA, Pal D, Ghosh A, et al. Impact of a-cations modified on the structural, electronic, optical, mechanical, and solar cell performance of inorganic novel A_3NCl_3 (A = Ba, Sr, and Ca) Perovskites. *Energy and Fuels*. 2024; 38(9): 8199-8217.
[6] Reza MS, Reza MS, Ghosh A, Rahman MF, Ramalingam J, Ahmed F, et al. New highly efficient perovskite solar cell with power conversion efficiency of 31% based on Ca_3NI_3 and an effective charge transport layer. *Optics Communications*. 2024; 561: 130511. Available from: https://doi.org/10.1016/j.optcom.2024.130511.
[7] Kumar M, Raj A, Kumar A, Anshul A. An optimized lead-free formamidinium Sn-based perovskite solar cell design for high power conversion efficiency by SCAPS simulation. *Optical Materials*. 2020; 108: 110213. Available from: https://doi.org/10.1016/j.optmat.2020.110213.
[8] Jahan N, Ghosh A, Ahmed F, Buian MFI, Al-Yousup M, Miazee AA, et al. A comparative study of CuO based solar cell with ZnTe HTL and SnS_2 ETL using SCAPS 1D simulation. *Journal of Optics*. 2024; 2024: 1-13. Available from: https://doi.org/10.1007/s12596-024-01800-6.
[9] Ghosh A, Bakkar A, Momina, Asmat N, Ahmed F, Buian MFI, et al. Enhancing solar cell efficiency beyond 27% through the implementation of an efficient charge transport layer utilizing an innovative inorganic perovskite Sr_3PI_3. *Journal of Physics and Chemistry of Solids*. 2024; 190: 112029. Available from: https://doi.org/10.1016/j.jpcs.2024.112029.
[10] Reza MS, Rahman MF, Kuddus A, Mohammed MKA, Al-Mousoi AK, Islam MR, et al. Boosting efficiency above 28% using effective charge transport layer with Sr_3SbI_3 based novel inorganic perovskite. *RSC Advances*. 2023; 13(45): 31330-31345.
[11] Pathak C, Pandey SK. Design, performance, and defect density analysis of efficient eco-friendly perovskite solar cell. *IEEE Transactions on Electron Devices*. 2020; 67(7): 2837-2843.
[12] Srivastava V, Chauhan RK, Lohia P, Yadav S. Achieving above 25% efficiency from $FA_{0.85}Cs_{0.15}Pb$ $(I_{0.85}Br_{0.15})_3$ perovskite solar cell through harnessing the potential of absorber and charge transport layers. *Micro and Nanostructures*. 2023; 184: 207691. Available from: https://doi.org/10.1016/j.micrna.2023.207691.
[13] Kumar M, Raj A, Kumar A, Anshul A. An optimized lead-free formamidinium Sn-based perovskite solar cell design for high power conversion efficiency by SCAPS simulation. *Optical Materials*. 2020; 108: 110213. Available from: https://doi.org/10.1016/j.optmat.2020.110213.
[14] Ritu, Gagandeep, Kumar R, Chand F. Optimization of ITO/SnO_2/$FASnI_3$/PCBM/Ag based perovskite solar cell. *Materials Today: Proceedings.* 2023. Available from: https://doi.org/10.1016/j.matpr.2023.05.690.
[15] Pachori S, Agrawal R, Choudhary BL, Verma AS. An efficient and stable lead-free organic-inorganic tin iodide perovskite for photovoltaic device: Progress and challenges. *Energy Reports*. 2022; 8: 5753-5763. Available from: https://doi.org/10.1016/j.egyr.2022.03.183.
[16] Moustafa M, Al Zoubi T, Yasin S. Numerical analysis of the role of p-$MoSe_2$ interfacial layer in CZTSe thin-film solar cells using SCAPS simulation. *Optik*. 2021; 247(7): 167885.
[17] Lang L, Yang JH, Liu HR, Xiang HJ, Gong XW. First-principles study on the electronic and optical properties of cubic ABX_3 halide perovskites. *Physics Letters A*. 2014; 378(3): 290-293.
[18] Azri F, Meftah A, Sengouga N, Meftah A. Electron and hole transport layers optimization by numerical simulation of a perovskite solar cell. *Solar Energy*. 2019; 181: 372-378. Available from: https://doi.org/10.1016/j.solener.2019.02.017.
[19] Pandey JK, Tauseef SM, Manna S, Patel RK, Singh VK, Dasgotra A. *Application of Nanotechnology for Resource Recovery from Wastewater*. USA: CRC Press; 2024.
[20] Jeon NJ, Noh JH, Yang WS, Kim YC, Ryu S, Seo J, et al. Compositional engineering of perovskite materials for high-performance solar cells. *Nature*. 2015; 517(7535): 476-480.
[21] Chen LC, Tseng ZL, Huang JK. A study of inverted-type perovskite solar cells with various composition ratios of $(FAPbI_3)_{1-x}(MAPbBr_3)x$. *Nanomaterials*. 2016; 6(10): 183.
[22] Ma FS, Li JW, Li WZ, Lin N, Wang LD, Qiao J. Stable α/δ phase junction of formamidinium lead iodide perovskites for enhanced near-infrared emission. *Chemical Science*. 2017; 8(1): 800-805.
[23] Zhou Y, Long G. Low density of conduction and valence band states contribute to the high open-circuit voltage in perovskite solar cells. *The Journal of Physical Chemistry C*. 2017; 121(3): 1455-1462.
[24] Gelvez-Rueda MC, Renaud N, Grozema FC. Temperature dependent charge carrier dynamics in formamidinium

lead iodide perovskite. *The Journal of Physical Chemistry C*. 2017; 121(42): 23392-23397.
[25] Karthick S, Velumani S, Bouclé J. Experimental and SCAPS simulated formamidinium perovskite solar cells: A comparison of device performance. *Solar Energy*. 2020; 205: 349-357. Available from: https://doi.org/10.1016/j.solener.2020.05.041.
[26] Gélvez-Rueda MC, Renaud N, Grozema FC. Temperature dependent charge carrier dynamics in formamidinium lead iodide perovskite. *The Journal of Physical Chemistry C*. 2017; 121(42): 23392-23397.
[27] Abdelaziz S, Zekry A, Shaker A, Abouelatta M. Investigating the performance of formamidinium tin-based perovskite solar cell by SCAPS device simulation. *Optical Materials*. 2020; 101: 109738. Available from: https://doi.org/10.1016/j.optmat.2020.109738.
[28] Du HJ, Wang WC, Zhu JZ. Device simulation of lead-free $CH_3NH_3SnI_3$ perovskite solar cells with high efficiency. *Chinese Physics B*. 2016; 25(10): 108802.
[29] Stamate MD. On the dielectric properties of dc magnetron TiO_2 thin films. *Applied Surface Science*. 2003; 218(1-4): 318-323.
[30] Saha P, Singh S, Bhattacharya S. $FASnI_3$-based eco-friendly heterojunction perovskite solar cell with high efficiency. *Micro and Nanostructures*. 2024; 186: 207739. Available from: https://doi.org/10.1016/j.micrna.2023.207739.
[31] Ball JM, Stranks SD, Hörantner MT, Huettner S, Zhang W, Crossland EJW, et al. Optical properties and limiting photocurrent of thin-film perovskite solar cells. *Energy & Environmental Science*. 2015; 8(2): 602-609.
[32] Mebarek-Oudina F. *EMS 2022*. 2022.
[33] Chehade G. *Recombination Dynamics and Excitonic Properties in 2D Hybrid Perovskites*. France: INIS Liaison Officer; 2022.
[35] Yang WS. *High-Quality Phase-Pure Formamidinium Perovskite Layers for Efficient Perovskite Solar Cells*. Ph.D. Thesis, Ulsan National Institute of Science and Technology; 2019.
[36] Kim JY, Lee JW, Jung HS, Shin H, Park NG. High-efficiency perovskite solar cells. *Chemical Reviews*. 2020; 120(15): 7867-7918.